Relaxation mechanisms of photoinduced periodic microstructures in ferrofluid layers

Dmitry Zablotsky* and Elmars Blums
Institute of Physics, Latvian University, Miera str. 32, Salaspils-1 LV-2169, Latvia
(Received 24 July 2011; published 8 December 2011)

We consider theoretically and numerically a periodic concentration grating induced in a layer of ferrofluid in the presence of the external magnetic field by nonuniform optical heating through photoabsorption. The stationary profiles of the periodic microstructures are governed by the equilibrium of the diffusive, thermodiffusive, and magnetic fluxes. The anisotropy of the diffusion coefficient and the magnetically driven microconvection contribute to the relaxation of these structures. The temperature-concentration coupling is shown to increase the initial effective diffusive relaxation rate by up to 50%. Microconvection dominates in the relaxation process even at small values of the control parameter and rapidly destroys the periodic part of the concentration grating. We describe this process in the weakly nonlinear regime by an approximate Galerkin model.

DOI: 10.1103/PhysRevE.84.066305 PACS number(s): 47.65.Cb, 47.20.−k, 42.65.Es

I. INTRODUCTION

Structurally ferrofluids are stable colloidal suspensions of ferromagnetic nanoparticles in liquid carrier. The huge difference in size and mass between the particles of the solid phase and the molecules of the solvent makes for the strong thermodiffusive coupling and as a consequence relatively large concentration differences in nonisothermal ferrofluids. Depending on the structure of the particle-solvent interface and the composition of the liquid carrier, either normal or anomalous thermodiffusion can be observed [1,2].

While the amplitude of the induced concentration perturbation can be significant, its dynamics is slow due to the small thermodiffusive mobility of the nanoparticles. The characteristic diffusion time scale is by several orders of magnitude larger than the thermal time scale, and the stationary concentration profile can be established only on relatively small length scales (up to several millimeters) in experimentally relevant time.

The diffusivity of the ferroparticles was observed to increase in the direction of the applied uniform magnetic field due to the magnetophoretic contributions in the self-magnetic field [3]. The formation of the periodic structures in ferrofluid layers by means of the photoabsorption and the relaxation of such structures is a convenient method of gaining understanding of the collective diffusion process of the magnetic nanoparticles both with and without the applied magnetic field.

Under some circumstances it is difficult to explain the relaxation process by the diffusive and magnetophoretic contributions alone, and it was shown that the convective stability of the relaxation stage may depend on the initial solutal Rayleigh number [4–6]. If the thickness of the ferrofluid layer is not very small, the transversal profile of the concentration field must be taken into account. Near-wall gradients, if large enough, may cause the appearance of the thresholdless parasitic microconvection with transversal convective currents. This type of microconvection may manifest in the stationary state as well.

II. PROBLEM FORMULATION

We consider a temperature grating induced in the $-y$ direction within an infinite layer of ferrofluid by a periodic heat source $\propto [1+\cos(\pi y)](1+r_c\delta c)$ describing the concentration-dependent absorption of the periodic incident intensity of light. The layer is enclosed between two horizontal solid sidewalls, which are impermeable to the concentration flux. The thickness of the ferrofluid layer corresponds to the period of the grating, and it is assumed that the heat flux through the sidewalls obeys Newton's law.

In response to the temperature grating the thermodiffusive coupling leads to the appearance of the corresponding concentration grating with the same periodicity (Fig. 1). For the sake of simplicity we consider only the anomalous Soret effect with the negative thermodiffusion constant. In this way the maxima and minima of the concentration distribution correspond to those of the temperature grating.

The formation of the concentration grating takes place within the uniform external magnetic field applied along the $-y$ axis, parallel to the gradient of the concentration. The demagnetizing fields induced within the layer become apparent in the magnetophoretic contributions to the effective diffusion coefficient and are capable of inciting convective motion through the magnetic body force.

Once the stationary state is established, the heating is stopped, and the relaxation of the temperature and concentration gratings takes place.

III. INITIAL STATE

The shape of the induced concentration grating is determined by the equilibrium of mass fluxes of ferroparticles due to regular diffusion, thermodiffusion, and the magnetophoresis in the self-magnetic field $\boldsymbol{j_c} = -\nabla\delta c - r_S\nabla\delta T + \mathcal{M}_{\rm ph}\nabla(\boldsymbol{h}\cdot\boldsymbol{\delta H})$ [7]:

$$0 = \Delta\delta T + \tau[1+\cos(\pi y)](1+r_c\delta c), \tag{1}$$

$$0 = \Delta[\delta c + r_S\delta T - \mathcal{M}_{\rm ph}(\boldsymbol{h}\cdot\boldsymbol{\delta H})], \tag{2}$$

$$\Delta\delta\psi = \tilde{\alpha}_c\nabla\cdot(\delta c\boldsymbol{h}), \tag{3}$$

$$\Delta\delta\varphi = 0. \tag{4}$$

*dmitrijs.zablockis@gmail.com

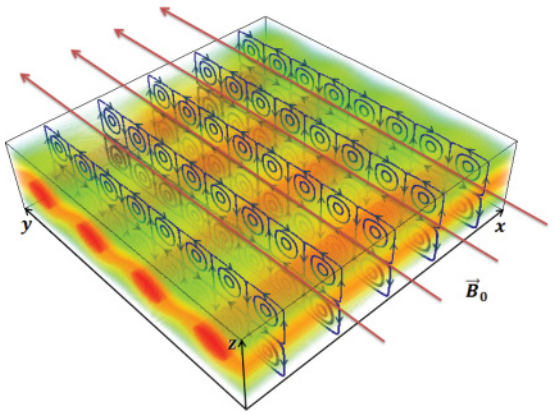

FIG. 1. (Color online) Definition of the problem: the concentration maxima of the optically induced concentration grating within the ferrofluid layer under the action of the applied uniform magnetic field. The transversal convective currents are incited by the magnetic forces.

The characteristic scales are the half-period L of the grating for the length, the diffusion scale $\frac{L^2}{D_c}$ for time, and Δc for the concentration. The concentration scale can be expressed through the amplitude of the initial temperature grating ΔT as $c_0(1-c_0)S_{\rm MT}\Delta T$, where $S_{\rm MT}$ is the effective magnetic Soret coefficient [7]. The relative strength of the magnetophoresis is governed by the magnetohoretic number $\mathcal{M}_{\rm ph}$, and $\tilde{\alpha}_c$ is the dimensionless specific magnetic susceptibility. The magnetization of the ferrofuid is assumed to depend mainly on the concentration and is directed along the applied field $\boldsymbol{\delta M} = [(1+\chi_0)\tilde{\alpha}_c\delta c]\boldsymbol{h}$. The parameter τ follows from the normalization of the temperature field and was taken as $\frac{1}{2}\pi^2 + \mathrm{Nu}^2$: the value determined from the solution of the one-dimensional problem in lateral $(-y)$ direction [7]. The coefficient $r_c = \frac{\Delta c}{c_0}$ determines the secondary absorption of the incident optical intensity.

The total magnetic scalar potential has been separated into purely internal $\delta\psi$ and external $\delta\varphi$ parts. Cyclic boundary conditions are imposed on all fields in the $-y$ direction to emulate the extent of the layer and periodicity of the grating. In the transversal $-z$ direction the induced heat is removed through the boundary condition of the third type; the solid phase, on the other hand, cannot penetrate the boundary, and the concentration flux is zero $[\boldsymbol{n}\,\boldsymbol{j_c} = 0]_{\partial S}$. Any possible deposition of the ferroparticles on the wall is neglected as well:

$$\left[\frac{\partial \delta T}{\partial \boldsymbol{n}} = -\mathrm{Nu}\cdot\delta T\right]_{\partial S}, \tag{5}$$

$$\left[\frac{\partial \delta c}{\partial \boldsymbol{n}} = -r_S\frac{\partial \delta T}{\partial \boldsymbol{n}} + \mathcal{M}_{\rm ph}\frac{\partial\,(\boldsymbol{h}\cdot\boldsymbol{\delta H})}{\partial \boldsymbol{n}}\right]_{\partial S}, \tag{6}$$

$$\left[\delta\psi = \delta\varphi,\ \frac{\partial\delta\psi}{\partial\boldsymbol{n}} = \frac{\partial\delta\varphi}{\partial\boldsymbol{n}}\right]_{\partial S}. \tag{7}$$

The boundary conditions for the magnetic scalar potential follow from the continuity of the normal and tangential components of the magnetic field $\delta H_\tau^{\rm in} = \delta H_\tau^{\rm out}$ and $\delta H_n^{\rm out} = \delta H_n^{\rm in} + \delta M_n^{\rm in}$.

We separate the variables and look for the solution to the system and boundary conditions in the following form up to the leading mode in the $-y$ direction:

$$\delta T_0(y,z) = t_0(z) + 2\cdot t_1(z)\cos(\pi y), \tag{8}$$

$$\delta c_0(y,z) = c_0(z) + 2\cdot c_1(z)\cos(\pi y), \tag{9}$$

$$\delta H_0(y,z) = 2\cdot h_1(z)\cos(\pi y). \tag{10}$$

Also, it is convenient to take the reference point at the center of the layer (with sidewalls at $z=\pm L$).

If the coefficient r_c is sufficiently small, the temperature and concentration equations become decoupled, and the solution is straightforward:

$$c_0(z) = \frac{\alpha_0}{p_0}z^2 - \frac{\tau r_s}{6},\quad c_1(z) = \alpha_0\mathrm{ch}(r_0 z) + \beta_0, \tag{11}$$

where the exponent is $r_0 = \sqrt{\lambda\pi^2}$ and

$$\alpha_0 = -b_0\beta_0,\quad \beta_0 = -\frac{\tau r_S}{2r_0^2},\quad \gamma_0 = \frac{\mathrm{Nu}}{f_0}\lambda\beta_0, \tag{12}$$

$$b_0 = \frac{1}{g_r}\left[\mathrm{Nu}\frac{g_0}{f_0} - \pi\,(\lambda-1)\right],\quad p_0 = \frac{b_0}{r_0^2}, \tag{13}$$

$$f_0 = \pi\,\mathrm{sh}\,(\pi) + \mathrm{Nu}\cdot\mathrm{ch}\,(\pi)\,, \tag{14}$$

$$g_0 = \pi\,\mathrm{sh}\,(\pi) + \pi\,\mathrm{ch}\,(\pi)\,,\quad g_r = r_0\,\mathrm{sh}\,(r_0) + \pi\,\mathrm{ch}\,(r_0) \tag{15}$$

with sh() and ch() denoting hyperbolic sines and cosines. Correspondingly, for the temperature and the magnetic field,

$$t_0\,(z) = -\frac{1}{r_S}\left[\frac{\alpha_0}{p_0}z^2 - \frac{\tau r_S}{\mathrm{Nu}}\left(1+\frac{\mathrm{Nu}}{2}\right)\right], \tag{16}$$

$$t_1\,(z) = -\frac{1}{r_S}\left[\lambda\beta_0 - \gamma_0\mathrm{ch}\,(\pi z)\right], \tag{17}$$

$$h_1\,(z) = \frac{1}{\mathcal{M}_{\rm ph}}\left[\alpha_0\mathrm{ch}\,(r_0 z) - (\lambda-1)\,\beta_0 + \gamma_0\mathrm{ch}\,(\pi z)\right]. \tag{18}$$

The obtained periodic profiles of the fields are plotted on Fig. 2. The concentration profile is slightly elongated in the lateral direction due to the magnetophoretic contributions and the anisotropy of the diffusion in the self-magnetic field. From (2) and (3) the effective diffusion coefficient in the direction of the applied field is $\frac{r_0^2}{\pi^2} = \lambda$ with $\lambda = 1 + \tilde{\alpha}_c\mathcal{M}_{\rm ph}$.

The magnetic force $\delta c\nabla\,(\boldsymbol{h}\cdot\boldsymbol{\delta H})$ is significantly nonuniform, and its components already allow us to predict the basic shape of the convective motion and the resulting deformation of the concentration field; microconvective rolls will compress the concentration grating in the $-z$ direction and enhance diffusive relaxation in the $-y$ direction.

When the coupling coefficient r_c cannot be neglected (i.e., the concentration perturbation is comparable with the initial concentration), the system (1)–(4) yields a characteristic equation with two exponents:

$$r_i^2 = \tfrac{1}{2}\left(r_0^2 + 2\tau r_S r_c \pm \sqrt{\Delta}\right),\quad \Delta = r_0^4 + 2\tau^2 r_S^2 r_c^2 \tag{19}$$

and the solution:

$$c_0\,(z) = \sum_i \frac{\alpha_i}{p_i}\mathrm{ch}\,(r_i z) - \frac{1}{r_c}, \tag{20}$$

$$c_1\,(z) = \sum_i \alpha_i\mathrm{ch}\,(r_i z), \tag{21}$$

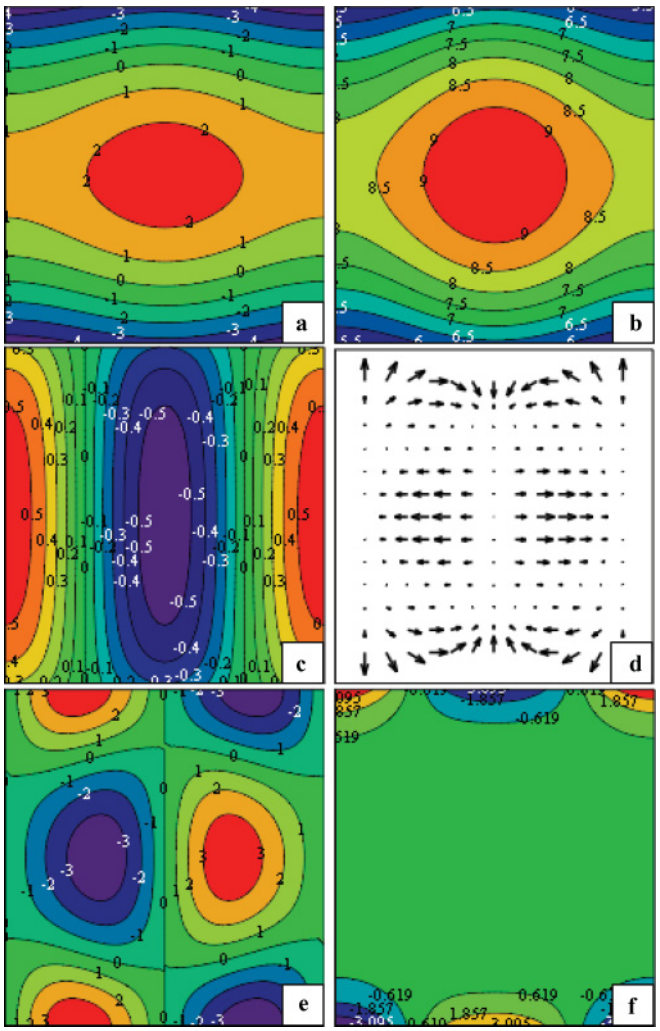

FIG. 2. (Color online) The stationary state of the concentration grating: (y-z) profiles of the perturbations of (a) concentration, (b) temperature, (c) lateral magnetic field $\boldsymbol{h}\cdot\boldsymbol{\delta H}$, (d) magnetic force $\delta c\nabla(\boldsymbol{h}\cdot\boldsymbol{\delta H})$, (e) lateral, and (f) transversal components of the magnetic force within a single period of the grating.

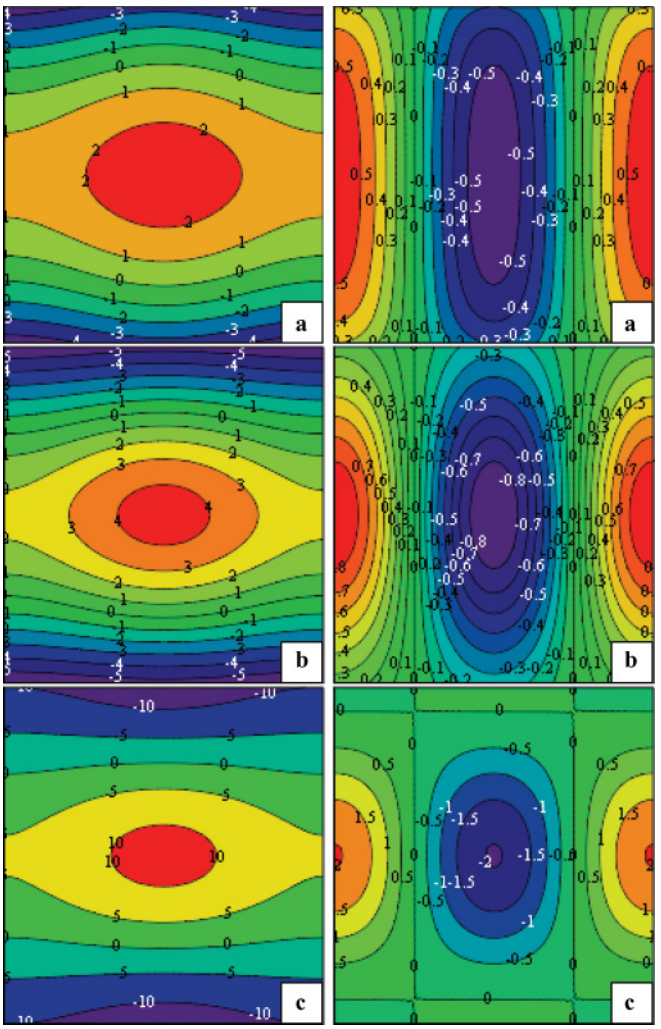

FIG. 3. (Color online) (y-z) profiles of the stationary concentration (left) and magnetic field (right) distributions within the layer at different values of the coupling parameter r_c: (a) $r_c = 0.0$, (b) $r_c = 0.25$, (c) $r_c = 0.5$.

$$t_0(z) = -\frac{1}{r_S}\left[\sum_i \frac{\alpha_i}{p_i}\mathrm{ch}(r_i z) - \lambda\right], \tag{22}$$

$$t_1(z) = -\frac{1}{r_S}\left[\sum_i \alpha_i d_i \mathrm{ch}(r_i z) - \gamma\,\mathrm{ch}(\pi z)\right], \tag{23}$$

$$h_1(z) = \frac{1}{\mathcal{M}_{\mathrm{ph}}}\left[\sum_i \alpha_i (1-d_i)\,\mathrm{ch}(r_i z) + \gamma\,\mathrm{ch}(\pi z)\right], \tag{24}$$

where $i = 1,2$. The other parameters are

$$p_i = \frac{r_i^2}{\tau r_S r_c} - 1, \quad d_i = \frac{r_i^2 - r_0^2}{r_i^2 - \pi^2}, \tag{25}$$

$$f_i = r_i\,\mathrm{sh}(r_i) + \mathrm{Nu}\cdot\mathrm{ch}(r_i), \tag{26}$$

$$g_i = r_i\,\mathrm{sh}(r_i) + \pi\,\mathrm{ch}(r_i), \tag{27}$$

$$b_i = \frac{1}{g_i(1-d_i) + \frac{g_0}{f_0} f_i d_i}, \tag{28}$$

$$\alpha_i = \pm\frac{1}{r_c}\frac{b_i}{\frac{b_1}{p_1}\frac{\mathrm{sh}(r_1)}{r_1} - \frac{b_2}{p_2}\frac{\mathrm{sh}(r_2)}{r_2}}, \tag{29}$$

$$\gamma = \frac{1}{f_0}\sum_i f_i d_i \alpha_i, \quad \lambda = \frac{1}{\mathrm{Nu}}\sum_i \frac{f_i}{p_i}\alpha_i. \tag{30}$$

Increasing the value of the coupling parameter r_c the concentration grating becomes sharper (Fig. 3). The intensity of the demagnetizing field increases within the layer and is attenuated outside. From the physical point of view higher values of the coupling parameter r_c mean enhanced absorption of heat due to the migration of the nanoparticles into the heated region, which in turn further increases the absorption of heat and the mass flux until countered by the diffusion and the magnetophoresis. The temperature distribution then becomes slightly elongated in the direction of the applied field due to the secondary absorption.

IV. DIFFUSIVE RELAXATION

Once the stationary state has been established, the heating is stopped and the grating is allowed to relax. The relaxation of the temperature grating is almost immediate owing to the smallness of the Lewis number $\mathrm{Le} = \frac{\chi}{D_c}$ characterizing the relation of time scales of the thermal and concentration diffusion ($\sim 10^{-4}$ in ferrofluids). The relaxation of the concentration grating is much slower and, discarding temperature, is described by the system of equations

$$\frac{\partial}{\partial t}\delta c = \Delta[\delta c - \mathcal{M}_{\mathrm{ph}}(\boldsymbol{h}\cdot\boldsymbol{\delta H})], \tag{31}$$

$$\Delta\delta\psi = \tilde{\alpha}_c \nabla\cdot(\delta c \boldsymbol{h}), \tag{32}$$

$$\Delta\delta\varphi = 0 \tag{33}$$

with the boundary conditions

$$\left[\frac{\partial\delta c}{\partial \boldsymbol{n}} = \mathcal{M}_{\mathrm{ph}}\frac{\partial(\boldsymbol{h}\cdot\boldsymbol{\delta H})}{\partial \boldsymbol{n}}\right]_{\partial S}, \tag{34}$$

$$\left[\delta\psi = \delta\varphi,\ \frac{\partial\delta\psi}{\partial \boldsymbol{n}} = \frac{\partial\delta\varphi}{\partial \boldsymbol{n}}\right]_{\partial S}, \tag{35}$$

and initial conditions in either (11) or (20)–(21) form. We again separate the spatial variables up to the leading mode in the lateral direction (9), but this time coefficients c_0 and c_1 depend on time. Because under the considered configuration of the applied field the perturbation of the magnetic field does not have zero-order lateral contribution, the coefficient c_0 has simple homogeneous Neumann boundary conditions and can be solved for by the Fourier method:

$$c_0(z,t) = \sum_{n=1}^{\infty} c_n(t)\cos(\pi n z), \tag{36}$$

$$c_n(t) = 2\cdot(-1)^n \sum_i \frac{\alpha_i}{p_i}\frac{r_i \mathrm{sh}(r_i)}{r_i^2 + (\pi n)^2} e^{-(\pi n)^2 t}. \tag{37}$$

The profile c_1, on the other hand, is most conveniently obtained by applying the unilateral Laplace transform $\hat{f}(s) = \mathcal{L}\{f(t)\} = \int_0^\infty e^{-st} f(t)\,dt$ to the problem. The solution in the complex s-domain is straightforward and

$$\hat{c}_1(z,s) = A(s)\mathrm{ch}[r(s)z] - \sum_i \frac{\alpha_i}{r_i^2 - r^2(s)}\mathrm{ch}(r_i z). \tag{38}$$

The coefficient $A(s) = \frac{\Phi(s)}{\Psi(s)}$ is determined from the boundary conditions and

$$\Phi(s) = -[(\lambda-1)\pi^2 + s]\sum_i \alpha_i \times \left[\left(\lambda\pi^2 - r_i^2\right) r_i \mathrm{sh}(r_i) - (\lambda-1)\pi^3 \mathrm{sh}(\pi)\frac{g_i}{g_0}\right] \times \left[r_i^2 - r^2(s)\right]\left(r_i^2 - \pi^2\right), \tag{39}$$

$$\Psi(s) = \left\{ s r(s)\mathrm{sh}[r(s)] + (\lambda-1)\pi^3 \mathrm{sh}(\pi)\frac{g_s(s)}{g_0}\right\} \times \prod_i \left(r_i^2 - \pi^2\right)\left[r_i^2 - r^2(s)\right], \tag{40}$$

where $r(s) = \sqrt{r_0^2 + s}$ and $g_s(s) = r_s(s)\mathrm{sh}[r_s(s)] + \pi\,\mathrm{ch}[r_s(s)]$.

To transform the solution back to the time domain we make use of the Vaschenko-Zakharchenko expansion for a function, which can be represented as a ratio of two generalized polynomials. The leading lateral modes of the concentration field and the magnetic field are then

$$c_1(z,t) = \sum_{n=1}^{\infty} \frac{\Phi(s_n)}{\Psi'(s_n)}\mathrm{ch}[r(s_n)z] e^{s_n t}, \tag{41}$$

$$h_1(z,t) = \frac{\tilde{\alpha}_c \pi^2}{g_0}\sum_{n=1}^{\infty} \frac{g_0 \mathrm{ch}[r(s_n)z] - g_s(s_n)\mathrm{ch}(\pi z)}{r^2(s) - \pi^2}\frac{\Phi(s_n)}{\Psi'(s_n)} e^{s_n t}, \tag{42}$$

where s_n are the roots of the transcendental expression[1]

$$\coth[r(s)] + \frac{r(s)}{\pi}\left[1 + \frac{s g_0}{(\lambda-1)\pi^3 \mathrm{sh}(\pi)}\right] = 0. \tag{43}$$

The obtained profiles of the concentration and the magnetic field are plotted on Fig. 4 at different stages of the relaxation process.

The mobility of the ferroparticles is the highest in the direction of the applied field due to anisotropy of the effective diffusion coefficient. We choose to express the effective lateral diffusion coefficient as

$$\lambda_{\mathrm{eff}} = -\frac{1}{\pi^2 J}\frac{\partial}{\partial t} J, \tag{44}$$

$$J(t) = \sqrt{\int_{-1}^{1}\left[\int_{-1}^{1}\delta c(y,z,t)\cos(\pi y)\,dy\right]^2 dz}. \tag{45}$$

When $r_c \to 0$, λ_{eff} would approach λ in the case of an unbounded layer. The dependence of λ_{eff} on time and the coupling coefficient r_c is shown on Fig. 5 in relation to λ.

We observe a slight decrease of the value of the effective lateral diffusion coefficient due to the presence of the transversal boundary conditions. The initial λ_{eff} noticeably increases as the coupling coefficient r_c is increased due to the additional accumulation of the magnetic nanoparticles resulting in the increase of the intensity of the demagnetizing field and the role of the magnetophoretic contributions. As the relaxation of the concentration grating progresses the diffusion coefficient approaches its value in the uncoupled case.

V. MICROCONVECTIVE RELAXATION

Nonhomogeneous magnetic forces induced within the volume of the ferrofluid layer by the external field cause the appearance of the microconvective motion, which may influence both the initial state and the relaxation process. For now we will assume the unperturbed initial distributions of the concentration and the magnetic field discussed above. The momentum conservation equation is added to the system (31)–(33):

$$D\delta c = \Delta[\delta c - \mathcal{M}_{\mathrm{ph}}(\boldsymbol{h}\cdot\boldsymbol{\delta H})], \tag{46}$$

$$\frac{1}{Sc} D\boldsymbol{u} = -\nabla p + \Delta\boldsymbol{u} + \mathrm{Rs}_m \delta c \nabla(\boldsymbol{h}\cdot\boldsymbol{\delta H}), \tag{47}$$

[1]While $s = -(\lambda-1)\pi^2$ is a root of $\Psi(s)$, it is also a root of $\Phi(s)$ and does not contribute to the solution.

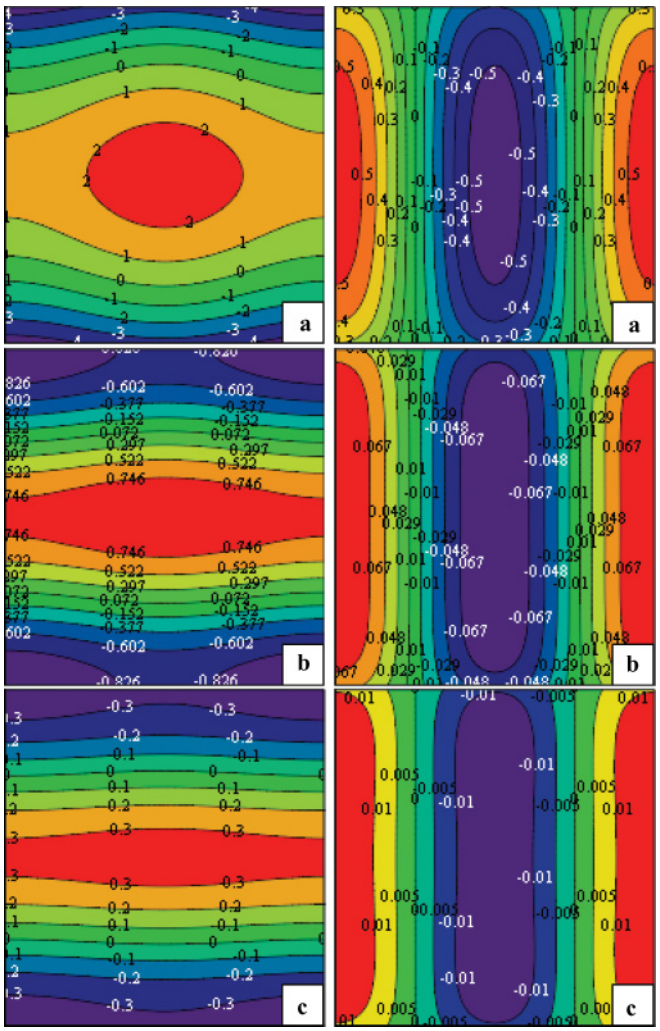

FIG. 4. (Color online) Diffusive relaxation of the concentration (left) and the corresponding magnetic field (right), (y-z) profiles sampled at (a) $t = 0.0$, (b) $t = 0.1$, (c) $t = 0.2$.

$$\Delta\delta\psi = \tilde{\alpha}_c \nabla \cdot (\delta c \boldsymbol{h}), \tag{48}$$

$$\Delta\delta\varphi = 0, \tag{49}$$

and the partial derivatives are replaced with the material derivative $D = [\frac{\partial}{\partial t} + (\boldsymbol{u_m} \cdot \nabla)]$. The boundary conditions for the magnetic scalar potentials remain the same (35), and we take advantage of the approximate boundary condition for the concentration $[\frac{\partial \delta c}{\partial \boldsymbol{n}} = 0]_{\partial S}$. The velocity boundary conditions are non-slip on the solid walls and $[\boldsymbol{u} = 0]_{\partial S}$ is implemented in the numerical simulations; however, for the sake of simplicity we use the free slip condition $[u_n = 0, \frac{\partial u_\tau}{\partial \boldsymbol{n}} = 0]_{\partial S}$ in the Galerkin problem. In many cases this approximation allows us to gain sufficient understanding of the convective patterns while significantly simplifying the coefficients of the solution. We retain only the basic modes and look for the solution in the following form:

$$u_z(y,z,t) = w_{11}(t)\cos(\pi y)\sin(\pi z), \tag{50}$$

$$\delta c(y,z,t) = \epsilon_{01}(t)\cos(\pi z) + \epsilon_{10}(t)\cos(\pi y) + \epsilon_{12}(t)\cos(\pi y)\cos(2\pi z). \tag{51}$$

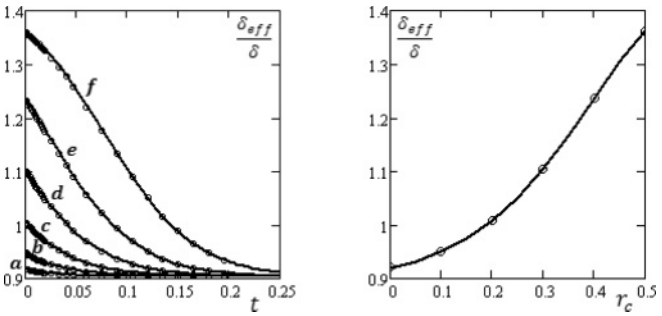

FIG. 5. Left: Dependence of the effective lateral diffusion coefficient $\lambda_{\text{eff}}(t)$ on time for different values of the coupling coefficient r_c: (a) $r_c = 0.0$, (b) $r_c = 0.1$, (c) $r_c = 0.2$, (d) $r_c = 0.3$, (e) $r_c = 0.4$, (f) $r_c = 0.5$. Right: Dependence of the initial effective lateral diffusion coefficient $\lambda_{\text{eff},0}(r_c)$ on the coupling coefficient r_c. Dots, numerical simulations; lines, analytical solution.

Inserting the ansatz (50)–(51) into the governing equations (46)–(49), projecting them onto the selected modes and taking into account that the Schmidt number is rather large in ferrofluids (Sc $\sim 10^4$–10^5), we obtain a three-mode Lorenz-type model for the determination of the mode amplitudes, which can be integrated by an appropriate time-stepping method. The equations for the three concentration perturbation modes:

$$\frac{\partial}{\partial t}\epsilon_{01} = -\pi^2\epsilon_{01} - \frac{\pi}{2}\left(\epsilon_{10} - \frac{\epsilon_{12}}{2} + 2\beta_0 e^{-r_0^2 t}\right), \tag{52}$$

$$\frac{\partial}{\partial t}\epsilon_{10} = -\lambda\pi^2\epsilon_{10} + \frac{\pi}{2}\left[c_1(t) + \epsilon_{01}\right] w_{11}, \tag{53}$$

$$\frac{\partial}{\partial t}\epsilon_{12} = -(\lambda+4)\pi^2\epsilon_{12} - \frac{\pi}{2}\left[c_1(t) - 3c_3(t) + \epsilon_{01}\right] w_{11}, \tag{54}$$

and the velocity mode can be expressed explicitly:

$$w_{11} = \frac{1}{4\pi}\cdot \mathrm{Rs}_m \Bigg\{ F_0(t) + [h_0(t) - h_2(t)]\epsilon_{01} + \tilde{\alpha}_c \Bigg[\frac{\mathrm{sh}(\pi)}{g_0}(\epsilon_{10} + \gamma_2\epsilon_{12})[c_1(t) + (1-\gamma_2)\epsilon_{01} + D(t)] - \epsilon_{10}[c_1(t) + \epsilon_{01}] + \frac{1}{2}\gamma_2\epsilon_{12}[c_1(t) - 3c_3(t) + \epsilon_{01}] \Bigg] \Bigg\}, \tag{55}$$

with $D(t) = \sum_{n=1}^{\infty}\gamma_n\left[(n+1)c_{n+1}(t) - (n-1)c_{n-1}(t)\right]$ and where $F_0(t) = \sum_{n=1}^{\infty} n c_n(t)\left[h_{n-1}(t) - h_{n+1}(t)\right]$ is the unperturbed magnetic force, and $c_n(t)$ and $h_n(t)$ are the respective Fourier expansion coefficients of $c_0(z,t)$ and $h_1(z,t)$.

Due to the initial nonuniformity of the concentration field and the resulting nonpotential magnetic force $F_0(t)$ the amplitude of the convective perturbation w_{11} rapidly adjusts and increases to its maximum value w_{11}^0, followed by the exponential relaxation. Solving (55) for the leading mode of the $F_0(t)$ expansion, we obtain

$$w_{11}^0 = \frac{2}{\pi^3}\tilde{\alpha}_c\beta_0\frac{\alpha_0}{p_0}\mathrm{Rs}_m\left[\frac{\mathrm{sh}(\pi)}{g_0} - 1\right]. \tag{56}$$

The initial amplitude of the convective perturbation is linear in relation to the solutal Rayleigh number Rs_m (Fig. 6).

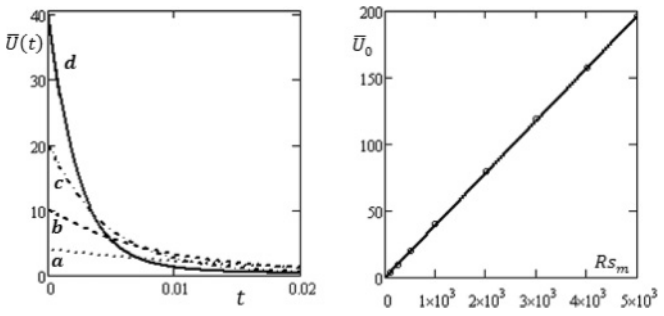

FIG. 6. Left: Relaxation of the averaged velocity magnitude $\bar{U}(t)$ at different values of the solutal Rayleigh number: (a) $\mathrm{Rs}_m = 100$, (b) $\mathrm{Rs}_m = 250$, (c) $\mathrm{Rs}_m = 500$, (d) $\mathrm{Rs}_m = 1000$. Right: Dependence of the averaged velocity amplitude $\bar{U}_0$ on the solutal Rayleigh number. Dots, numerical simulations; line, Galerkin solution.

The Galerkin model allows us to calculate the effective relaxation rate of the concentration perturbation (45) and is in good agreement with the results of the numerical simulations (Fig. 7); in fact, the correspondence is greatly improved as the relaxation of the grating progresses into the regular regime, because the higher modes relax much faster than the leading ones (37). We see that microconvection plays indeed a very significant role in the relaxation of the grating even at relatively low values of the solutal Rayleigh number Rs_m. At higher values of Rs_m the effective diffusion coefficient remains relatively unchanged over most of the relaxation process and exceeds the one for the purely diffusive relaxation approximately 2.7 times.

The evolution of the concentration grating (Fig. 8) is very similar to the purely diffusive case: The periodic part of the concentration perturbation c_1 quickly relaxes, forming a layer with increased nanoparticle concentration, followed by the slow relaxation of the resulting constant component c_0 of the perturbation. However, microconvection destroys the periodic grating much faster than the anisotropy of the diffusion coefficient.

VI. DISCUSSION

In thin ferrofluid layers the microconvective fluxes are induced within the plane of the layer via a stationary convective

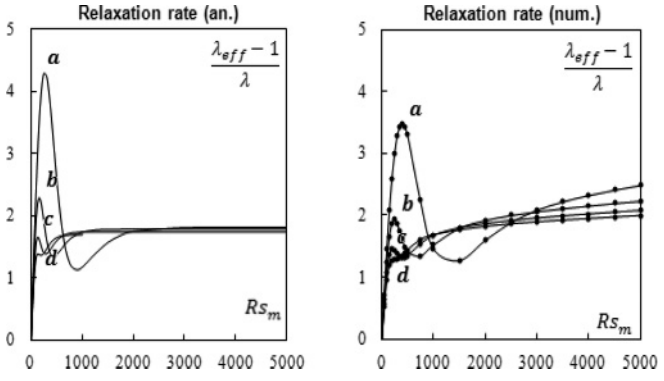

FIG. 7. Dependence of the relative effective latter relaxation rates λ_{eff} on the solutal Rayleigh number sampled at different times: (a) $t = 0.005$, (b) $t = 0.01$, (c) $t = 0.015$, (d) $t = 0.02$. Left: Galerkin solution; right: numerical simulations.

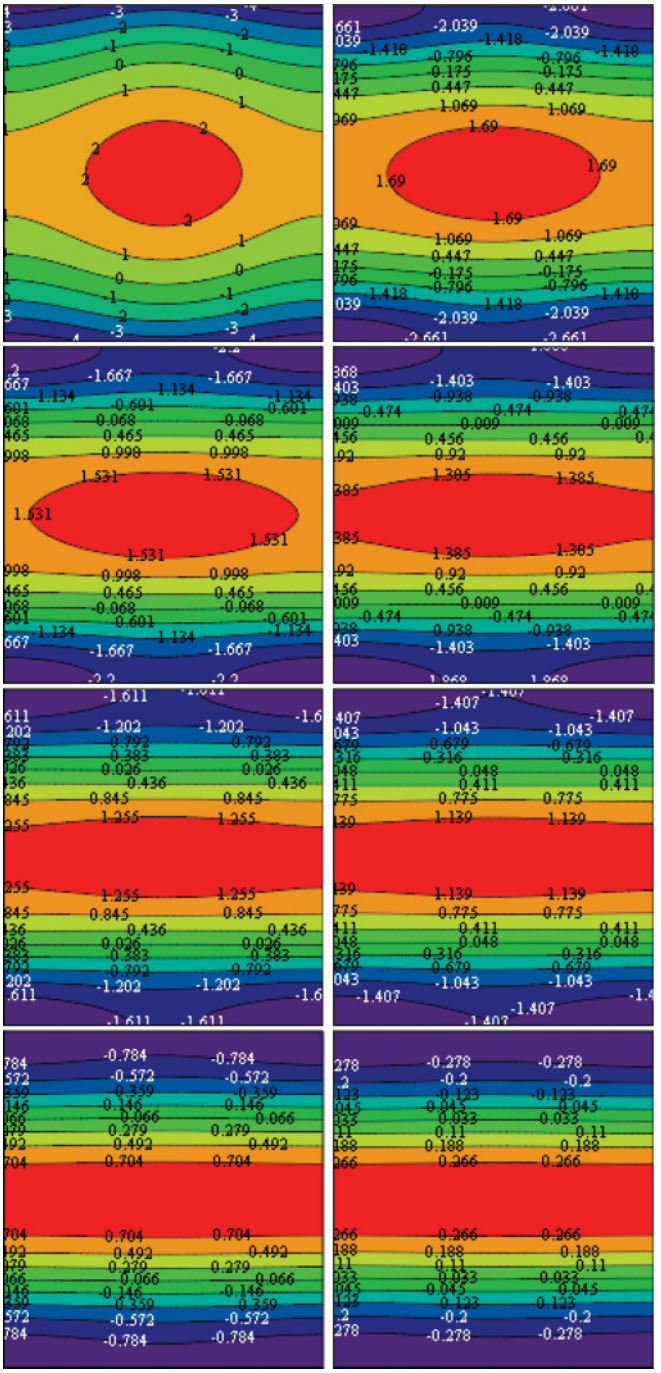

FIG. 8. (Color online) Evolution of the (y-z) profile of the concentration perturbation at different stages of the relaxation process for the solutal Rayleigh number $\mathrm{Rs}_m = 100$. Top: $t = 0.0, 0.01, 0.02, 0.03$; bottom: $t = 0.04, 0.05, 0.1, 0.2$ (Galerkin solution).

instability above the critical parameter and may destroy the uniformity of the concentration grating [8] when the optical pumping is switched off. There is indeed experimental evidence that both the relaxation time and the character of the relaxation process of the photoinduced concentration grating in the applied magnetic field depend on the thickness of the ferrofluid layer [9], which is contrary to the assumption of the two-dimensional relaxation regime and the diffusion and magnetophoresis in the self-magnetic field as the only

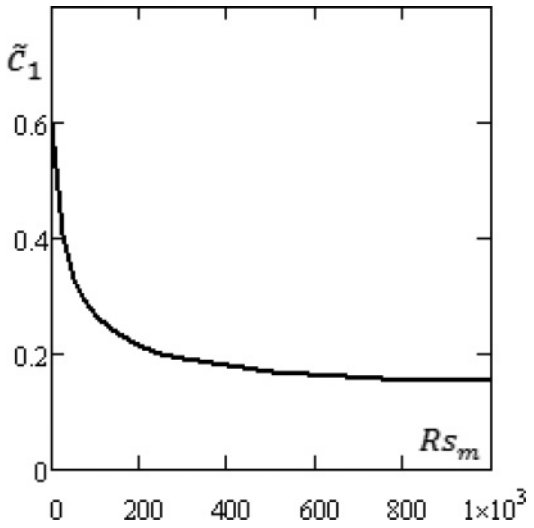

FIG. 9. Convective attenuation of the stationary amplitude of the first lateral mode $\tilde{c}_1$ of the concentration grating increasing the solutal Rayleigh number Rs_m (Galerkin solution).

contributing effects. Dependence of the stationary state of the concentration grating on the thickness of the layer has also been observed experimentally. While the former effect may suggest the presence of microconvective instability, the latter is characteristic of the threshold-less parasitic microconvection caused by the transversal gradients of the concentration and the demagnetizing field. The smearing of the stationary profile of the concentration field by convective fluxes leads to the attenuation of the stationary concentration amplitude and the visibility of the grating (Fig. 9). The intensity of the parasitic magnetoconvection may be decreased by increasing the aspect ratio $\frac{L}{h}$ (interfringe to the thickness of the layer) of the photoinduced structures and decreasing the thickness of the layer but cannot be completely suppressed if the aspect ratio is not too large. Increasing the thickness of the layer, the transversal concentration profile determines as well the relaxation regime of the photoinduced periodic structures in the laterally applied uniform magnetic field. The presence of microconvection heavily influences the relaxation process contributing to the increase of the effective diffusion coefficient in the lateral direction many times as compared to the diffusive and magnetophoretic relaxation. While this type of microconvection does not influence the uniformity of the induced grating at reasonable values of the solutal Rayleigh number, the uniform convective rolls (50) become unstable at higher values of Rs_m leading to the appearance of fluxes in the $-x$ direction along the extent of the grating.

ACKNOWLEDGEMENT

This work has been supported by the European Social Fund within the project Support for Doctoral Studies at University of Latvia.

[1] T. Voelker, E. Blums, and S. Odenbach, Magnetohydrodynamics **37**, 274 (2001).
[2] J. Lenglet, A. Bourdon, J. C. Bacri, and G. Demouchy, Phys. Rev. E **65**, 031408 (2002).
[3] J. C. Bacri, A. Cebers, A. Bourdon, G. Demouchy, B. M. Heegaard, B. Kashevsky, and R. Perzynski, Phys. Rev. E **52**, 3936 (1995).
[4] A. Cebers and M. Igonin, Magnetohydrodynamics **38**, 455 (2004).
[5] M. Igonin, Magnetohydrodynamics **40**, 53 (2004).
[6] A. Mezulis and E. Blums, J. Non-Equilibrium Thermodynamics **32**, 331 (2007).
[7] D. Zablotsky and E. Blums, JMMM **323**, 1338 (2011).
[8] D. Zablotsky and E. Blums, Phys. Rev. E **84**, 026319 (2011).
[9] A. Mezulis and E. Blums, Magnetohydrodynamics **40**, 337 (2004).